Caren Gatzen\*, Daniel Emil Mack, Olivier Guillon, Robert Vaßen

c.gatzen@fz-juelich.de, d.e.mack@fz-juelich.de, o.guillon@fz-juelich.de, r.vassen@fz-juelich.de

\* Corresponding Author: c.gatzen@fz-juelich.de

Forschungszentrum Jülich GmbH, Institute of Energy and Climate Research,
Materials Synthesis and Processing (IEK-1), 52425 Jülich, Germany

## Water Vapor Corrosion Test Using Supersonic Gas Velocities

Testing of the corrosion resistance of *environmental barrier coating* (EBC) systems is necessary for developing reliable coatings. Unfortunately tests under realistic gas turbine conditions are difficult and expensive. The materials under investigation as well as parts of the test setup have to withstand high temperatures (≥ 1200 °C), high pressure (up to 30 bar) as well as the corrosive atmosphere (H<sub>2</sub>O, O<sub>2</sub>, NO<sub>8</sub>). Therefore most lab scale test-rigs focus on simplified test conditions. In this work water vapor corrosion testing of EBCs with a HVOF (*high velocity oxy fuel*) facility is introduced which combines high temperatures and high gas velocities. It leads to quite high recession rates in short periods of time, which are comparable to results from literature. It was found that high flow velocities can easily compensate low gas pressures. HVOF-testing is a simple and fast way to measure the recession rate of an EBC-system. As proof of concept the recession rates of an oxide/oxide CMC with and without EBC were measured.

# **List of Symbols**

 $D_{AB}$  Diffusion coefficient of A in B

F Flux

 $\Delta_r G^{\circ}$  Free reaction enthalpy

 $\eta$  Dynamic viscosity

JAI(OH)3 Mass transport of Al(OH)3

L Characteristic length

M Molar mass

*v* Kinematic viscosity

*p*<sub>H2O</sub> Water vapor partial pressure

 $p_{\text{total}}$  Total pressure

R Ideal gas constant

*Re* Reynolds number

Sc Schmidt number

Sh Sherwood number

*T* Temperature

*ν* Gas velocity

# List of acronyms

APS Atmospheric plasma spraying

BET Brunauer-Emmet-Teller theory, surface measurement technique

CEA Chemical equilibrium with applications

CMC Ceramic matrix composite

EBC Environmental barrier coating

EDX Energy-dispersive X-ray spectroscopy

HVOF High velocity oxy fuel

SEM Scanning electron microscopy

slpm standard liters per minute

YSZ Yttria-stabilized zirconia

### Introduction

Since gas turbines were introduced both in aircraft engines and for power generation, there has been a constant search for further efficiency increases. An increase in efficiency of aero engines could be achieved, for example, by increasing the pressure ratio or increasing the operating temperature.<sup>[1]</sup> A step forward can be made by the use of new base materials with improved high temperature capabilities.[1] Currently SiC fiber/SiC matrix composites and oxide fiber/oxide matrix composites (mainly Al<sub>2</sub>O<sub>3</sub>) are candidates for hydrocarbon fueled turbine applications at hot stage parts. [1-6] Since Al<sub>2</sub>O<sub>3</sub> is an oxide ceramic, it is very resistant to oxidation<sup>[7-9]</sup>, while SiC tends to oxidize at high temperatures and form a SiO<sub>2</sub> protective layer on the surface. Despite that, SiC based CMCs are often preferred because of their superior creep properties. However, the high temperature part of a gas turbine comprises an aggressive atmosphere of combustion gases to which the components are exposed. Depending on the fuel, the composition varies. The main combustion products of hydrocarbon fueled turbines are CO<sub>2</sub> and H<sub>2</sub>O, while hydrogen fueled turbines and rockets mainly form H<sub>2</sub>O. The water vapor attacks the components and forms volatile hydroxides[10-13] (see equations 1-3), this leads to a continuous loss of material. Compared to SiC, Al<sub>2</sub>O<sub>3</sub> is much more corrosion-resistant.

$$2 \, SiC + 3 \, O_2 \rightarrow 2 \, SiO_2 + 2 \, CO$$
 (1)

$$3 SiO_2 + 6 H_2 O \rightarrow 3 Si(OH)_4$$
 (2)

$$Al_2O_3 + 3H_2O \rightarrow 2Al(OH)_3$$
 (3)

In general, the mass transport ( $J_A$ ) of species A through fluid B is defined in equation 4. The mass loss is dependent on the diffusion coefficient of A in B ( $D_{AB}$ ), the molar mass (M), the partial pressure ( $p_A$ ), the characteristic length of the sample (L), the ideal gas constant (R), the temperature (T) and the Sherwood-number (Sh). The Sherwood number can be approximated by a function of the Reynolds- (Re) and Schmidt- (Sc) number. The Reynolds-number describes the ratio of inertial forces to viscous forces, it is dependent on the density ( $\rho$ ), velocity ( $\nu$ ) and viscosity ( $\eta$ ) of the fluid as well as the characteristic sample length. The Schmidt-number is the ratio of kinematic viscosity and mass diffusivity. There are two cases: laminar and turbulent (see equations 5&6).

$$J_A = Sh \cdot \frac{D_{AB} \cdot M_A \cdot p_A}{L \cdot R \cdot T} \tag{4}$$

$$J_A \approx 0.664 \cdot Re^{1/2} \cdot Sc^{1/3} \cdot \frac{D_{AB} \cdot M_A \cdot p_A}{L \cdot R \cdot T}$$
 laminar (5)

$$J_A \approx 0.0365 \cdot Re^{4/5} \cdot Sc^{1/3} \cdot \frac{D_{AB} \cdot M_A \cdot p_A}{L \cdot R \cdot T}$$
 turbulent (6)

with 
$$Re = \frac{\rho_B \cdot v_B \cdot L}{\eta_B}$$
 and  $Sc = \frac{\eta_B}{\rho_B \cdot D_{AB}}$  (7-8)

The partial pressure of species A can be expressed as function of the density of the volatile species ( $\rho_A$ ), the partial pressure of the corrosive medium ( $p_{H2O}$ ,  $p_{O2}$ ) and the free reaction enthalpy ( $\Delta G$ ). The coefficients n and m depend on the present reaction stoichiometry. In the case of Al<sub>2</sub>O<sub>3</sub>,  $p_{O2}$  can be neglected because the material is already completely oxidized, leaving only  $p_{H2O}$  to be considered. Following equation 3 n is defined as 3/2.

$$p_{A} = \frac{R \cdot T \cdot \rho_{A}}{M_{A}} = p_{H_{2}O}^{n} \cdot p_{O_{2}}^{m} \cdot e^{-\Delta G/R \cdot T}$$
(9)

By combining the equations shown above, a simplified dependence for the mass transfer for aluminum hydroxide is given by (10&11)<sup>[15-16]</sup>.

$$J_{Al(OH)_3} \propto \frac{v^{1/2}}{P_{total}^{1/2}} \cdot P_{H_2O}^{3/2} \cdot e^{-\frac{\Delta_T G^0}{R \cdot T}}$$
 laminar (10)

$$J_{Al(OH)_3} \propto \frac{v^{4/5}}{P_{total}^{1/5}} \cdot P_{H_2O}^{3/2} \cdot e^{-\frac{\Delta_r G^0}{R \cdot T}}$$
 turbulent (11)

Environmental barrier coatings (EBCs) are used to protect the materials from corrosion reactions. These ceramic coatings are often applied by atmospheric plasma spraying (APS). For the selection of the coating material, attention is mainly paid to high temperature stability and corrosion resistance. Since the coatings and the CMCs (especially the oxidic ones) have rough and porous surfaces, the corrosion properties of the coating-substrate systems cannot be directly inferred from those of the bulk materials. Therefore, it is essential to study the performance of the real coating-substrate system.

Lab scale reproduction of the harsh conditions in real gas turbines require both, great financial and technical effort. Corrosion tests have been performed by different groups, but most of them focus on simplified tests at lower pressures and/or flow velocities.<sup>[10, 12-13, 15, 17-24]</sup> All tests have in common that extremely long test durations between 20 and 500 hours had to be used to measure relevant corrosion rates. This is another factor that makes these tests extremely expensive and time consuming.

According to equations 10 and 11, the mass transport is governed by the pressure, the water vapor partial pressure and the gas velocity. These parameters need to be changed to drastically shorten the test time. Hence, this study aims to utilize an HVOF-facility (high velocity oxy fuel), to develop a test procedure for the screening of different materials in less than one hour by using supersonic gas velocities. Samples of an alumina-based CMC and Y<sub>2</sub>O<sub>3</sub>-coated samples of this CMC were used to demonstrate the feasibility of the test procedure.

.

# **Experimental Methods**

The used oxide CMC material was manufactured by *Walter E. C. Pritzkow Spezialkeramik, Filderstadt-Sielmingen* (*FW12*). The material consists of alumina fibers in a porous alumina matrix with additional 15 % 3YSZ.<sup>[25]</sup> The button type specimen had dimensions of 2.8 mm x 32 mm diameter. The corrosion behavior of the porous Al<sub>2</sub>O<sub>3</sub>-based CMC was compared to the corrosion properties of relatively dense Y<sub>2</sub>O<sub>3</sub>-EBCs. For this, some CMC samples were coated with Y<sub>2</sub>O<sub>3</sub> using Atmospheric Plasma Spraying (APS). The used *Multicoat* facility (*Oerlikon Metco, Switzerland*) was equipped with a *TriplexPro-210*<sup>TM</sup> gun mounted on a six-axis robot. For the coating process a commercially available Y<sub>2</sub>O<sub>3</sub> powder, with an average particle size of 30 μm, from *Oerlikon Metco, Switzerland* was used. The as sprayed coatings consisted of crystalline Y<sub>2</sub>O<sub>3</sub> with a coating thickness of around 240 μm.

Table 1: Properties of used CMC.[26]

Fiber	Nextel 610/1500 denier (DF11)	
Matrix	85% Al2O3 / 15% 3YSZ	
Fiber volume content	35-45 %	
CTE (25-1100 °C)	8,49 ·10 <sup>-6</sup> K <sup>-1</sup>	
Porosity	29 %	
Density	2.88 g⋅cm <sup>-3</sup>	
Thermal conductivity (300-1100 °C)	3.80-2.02 W·mK <sup>-1</sup>	

The HVOF corrosion tests were carried out in the same *Multicoat* facility. A DJ2600<sup>TM</sup> high velocity oxy-fuel (HVOF) gun was used for this purpose. Tests were

carried out by using hydrogen and oxygen in stoichiometric amounts as combustion gases and therefore simulating the water vapor content in turbine environments. In general, it would be possible to use methane or kerosene as fuel to simulate the combustion atmosphere of a hydrocarbon fueled turbine more extensively. Nitrogen was used as sheath gas. The test setup is illustrated in Figure 1. The test conditions are shown in Table 2. The specimen temperature was measured head on by a long wavelength infrared pyrometer ( $\lambda = 10 \mu m$ ) and on the back by a thermocouple (PtRh-Pt) which was thermally insulated against convection cooling on the backside and clamped between sample and holder. To optimize the flow conditions, [27-28] the sample was inclined by 45° with respect to the jet axis. The specimen temperature was controlled by changing the stand-off distance to the gun. The distance was adjusted in a way that temperatures of around 1470 K on the backside and 1670 K at the front were obtained. All experiments were carried out at least twice. Each sample was weighted and its surface was scanned by white light interferometry (cyberTechnologies, Eching, CT350T) before and after the test.

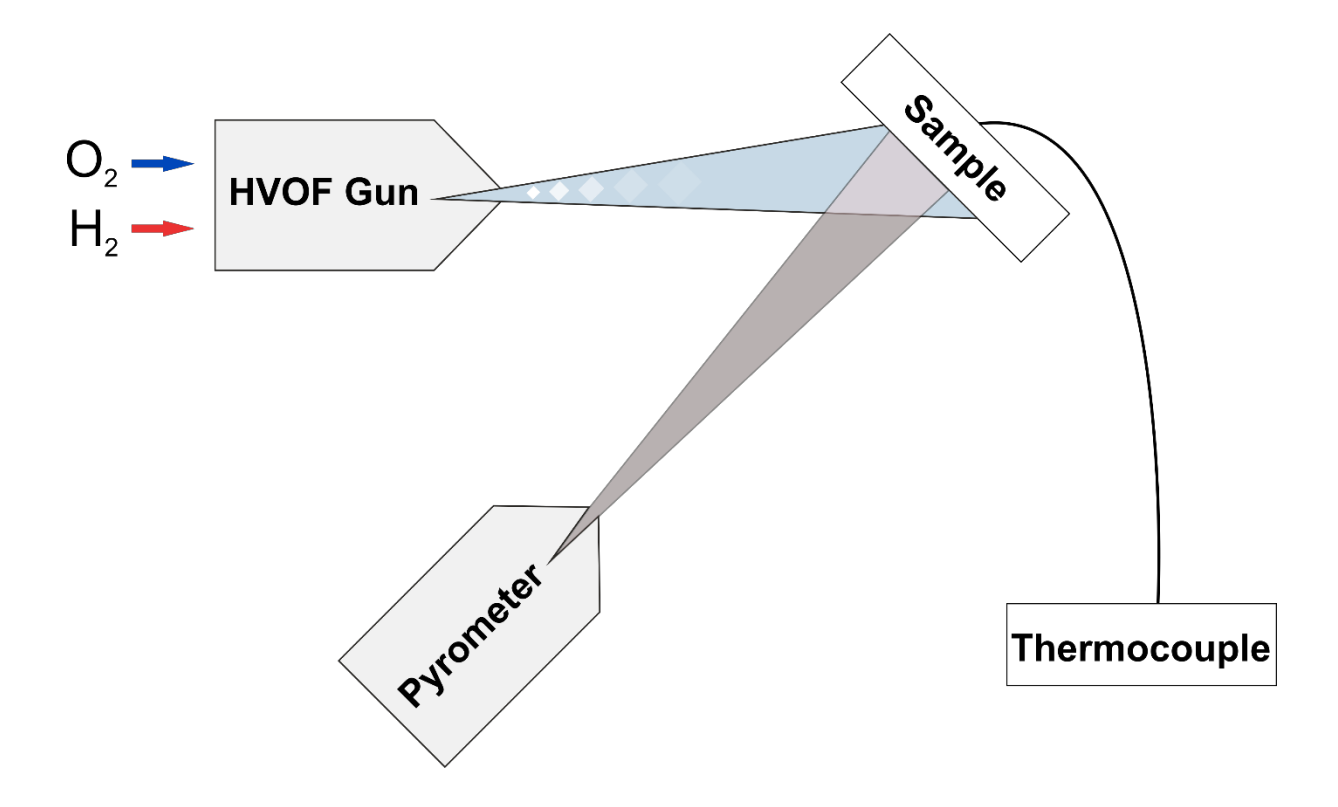


Figure 1: Schematic test setup of HVOF corrosion test, sample inclined by 45° with respect to the gun axis.

The composition of the corrosive combustion atmosphere and the gas velocity were calculated applying the software code *Chemical Equilibrium with Applications* (CEA) from NASA<sup>[29-30]</sup>. Although the expansion through the nozzle is calculated just one-dimensionally and turbulence effects are not considered, it can be used to estimate the test conditions as well as the completeness of the combustion. It was assumed that the total pressure at the sample position is atmospheric.

Table 2: Test parameters of HVOF-tests.

Distance	170 - 180 mm
T Front	1670 K
T Back	1470 K

Sheathing Gas Flow	460 slpm
Oxygen Flow	345 slpm
Hydrogen Flow	693 slpm

Corrosion induced changes of the composition and microstructure of the specimen were further characterized by means of X-ray diffraction (XRD) and scanning electron microscopy (SEM). XRD measurements were carried out, using a Bruker D4 Endeavor with Cu-K $\alpha$ -radiation ( $\lambda$  = 1.54187 Å). For the measurements after the test the grazing incident technique (1°) was used to measure only the surface composition of the sample. The penetration depth was in the range of 1  $\mu$ m. For these measurements an Empyrean ( $Malvern\ Panalytical,\ Netherlands$ ) using parallel beam optics was used. The Rietveld refinements were carried out with TOPAS V4 ( $Bruker\ AXS,\ Karlsruhe,\ Germany$ ).

The accessible surface area of the CMC was determined by nitrogen physisoption (BET measurements). Therefore, an *AREAMAT* from *JUNG INSTRUMENTS GmbH* (Germany) was used. Materialographic cross sections of samples before and after the testing were prepared. For this, the samples were sputtered with Pt and then galvanically nickel plated prior to embedding. Afterwards the samples were cut and wet ground with successively finer abrasive paper down to a grit designation of P4000. Afterwards the samples were polished with diamond suspensions.

### **Results & Discussion**

#### **Corrosion Conditions**

Calculations were made to estimate the water partial pressure, the gas flow velocity and temperature. The gas flow at the nozzle and at the sample was calculated, assuming a total pressure of 0.1 MPa at sample position. The gas velocity was calculated to be 2622 m·s·¹ at the nozzle exit and 2243 m·s·¹ where the gas expanded to 0.1 MPa, which is almost twice as much as the speed of sound at the present gas temperature (2802 K). It is assumed that the flow velocity at the sample position lies in between these values. The results show that the water vapor partial pressure at the sample position is around 69 kPa.

According to equation 1 and 2, for a given temperature and flow velocity, total pressure and water vapor partial pressure have major impact on the corrosion rate. In search for a factor to compare the various test facilities, this dependency , in the following referred to as flux  $(F)^{[15]}$ , was used. The flux of each test facility was calculated for laminar and turbulent regime, according to equation 12 and 13, by neglecting different test temperatures.

$$F \propto \frac{v^{1/2}}{P_{total}^{1/2}} \cdot P_{H_2O}^{3/2} \qquad \text{Laminar flow} \qquad (12)$$

$$F \propto \frac{v^{4/5}}{P_{total}^{1/5}} \cdot P_{H_2O}^{3/2}$$
 Turbulent flow (13)

The calculated fluxes of the different test facilities were calculated for the hypothetical laminar and turbulent case and plotted against the total pressure and flow velocity in a full logarithmized diagram (Figure 2). It is noticeable that at low flow velocities the laminar case achieves higher corrosion rates, while at higher velocities the turbulent flow will lead to higher corrosion rates. From this collection of data it seems that the flow velocity has major impact on the flux. Therefore, F was plotted as function of the flow velocity (see Figure 3). The nearly linear trend and the intersection of laminar and turbulent flow at x=0.7833, y=0.6415 can be clearly seen. This indeed shows that for low gas velocities a laminar flow leads to higher mass loss, while for high velocities a turbulent flow has the most impact. Consequently, to measure high rates in a short period of time, test rigs that operate at low gas velocities should make sure that a laminar flow is present, while facilities operating at high velocities should work in turbulent regime. This is often achieved due to the velocity dependence of the transition from laminar to turbulent flow.

According to equation 12 and 13 the water vapor partial pressure has the largest impact on the flux. But for technical reasons, the pressure can only be varied in a limited range, while the accessible range of the velocity does include several orders of magnitude ( $5\cdot10^{-4}$  to  $2\cdot10^{3}$  m·s<sup>-1</sup>). Therefore, it might be reasonable to compensate low partial pressures by high gas velocities. Figure 2 shows that a relatively low pressure can be easily compensated by a higher flow velocity. The test device presented in this paper shows the highest flux, although it operates at atmospheric pressure.

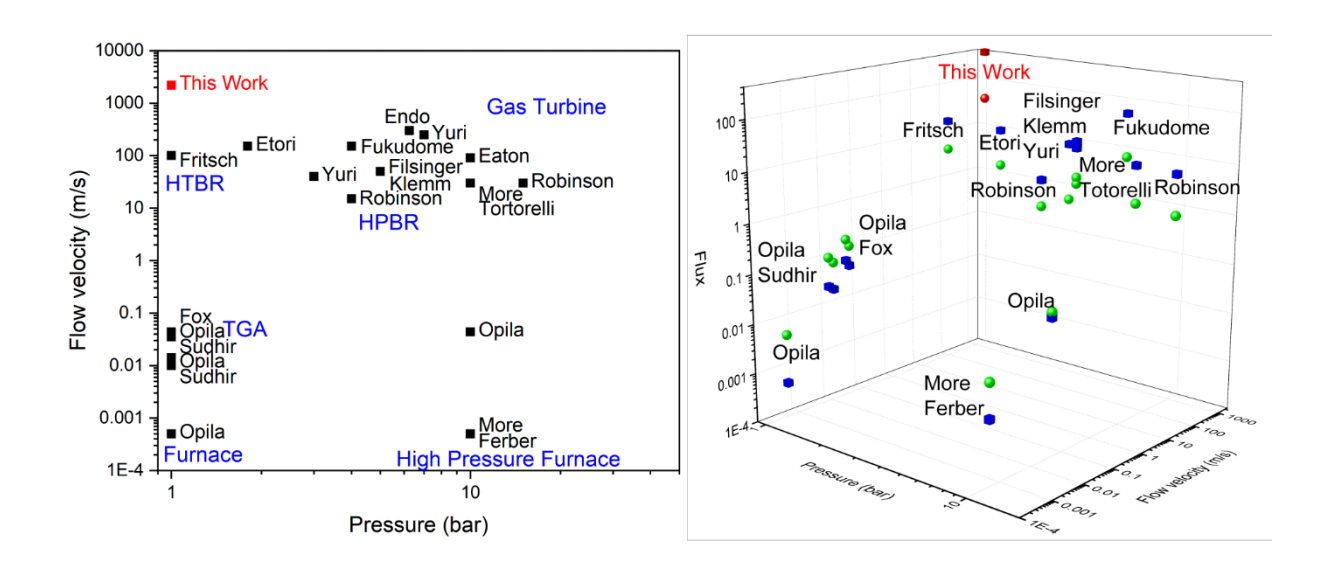


Figure 2: Overview on literature known corrosion test compared to this

work (left), three dimensional illustration including the flux

(right, green balls: laminar flow, blue cubes: turbulent flow).[11, 1519, 24, 31-43]

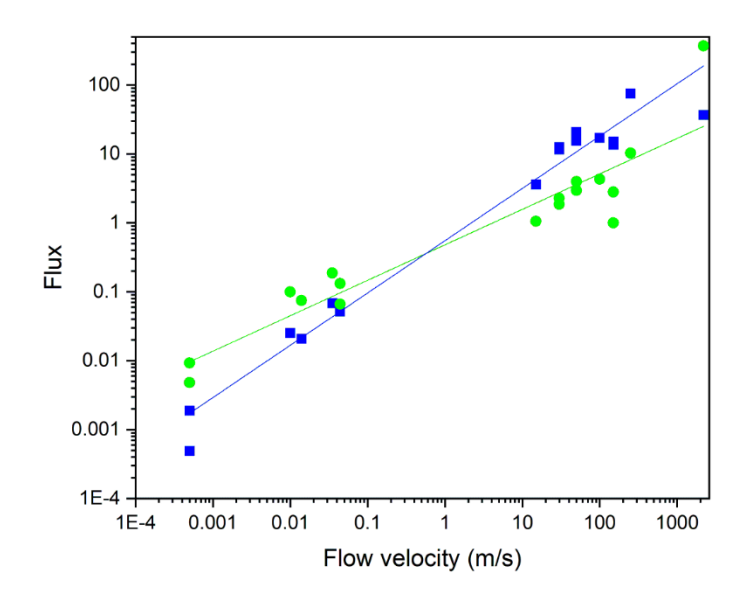


Figure 3: Flux as function of flow velocity (green circles: laminar flow, blue squares: turbulent flow).

The expected corrosion rates were calculated according to equations 5 and 6. The used values are tabulated in Table 3. The gas concentration of the water vapor steam (ρ) was calculated using the ideal gas law and the results of the CEA calculations. The equilibrium concentration of the volatile species (ρ') was calculated using the Al(OH)<sub>3</sub> partial pressure obtained from OPILA et al.<sup>[11]</sup> in combination with the ideal gas law. ρ' for Y<sub>2</sub>O<sub>3</sub> was estimated using the ideal gas law according to GOLDEN et al.<sup>[27]</sup> The specimens' radii were used as characteristic length (*L*). The viscosity of the fluid was tabulated by B. LATTO<sup>[44]</sup>. The diffusion coefficient (D<sub>AB</sub>) was calculated from the Chapman-Enskog equation<sup>[45]</sup>, using the tabulated values for the force constant, the collision diameter and the collision integral for H<sub>2</sub>O and the volatile species from SVEHLA et al.<sup>[46]</sup> For the hydroxides (Y(OH)<sub>3</sub>, Al(OH)<sub>3</sub>) this data cannot be found in literature, therefore the values of the halides AlF<sub>3</sub> and AlCl<sub>3</sub>, respectively, were used. According to KRIKORIAN<sup>[47]</sup> this approximation is valid, as hydroxides are

known to act as pseudo halides. The calculated recession rates are shown in Table 3. The calculated recession rates for turbulent flow are almost twice as high as the ones for the laminar flow. The calculated recession rate for Al<sub>2</sub>O<sub>3</sub> is two orders of magnitude higher compared to the calculated rates for Y<sub>2</sub>O<sub>3</sub>. GOLDEN et al.<sup>[27]</sup> did these calculations for Y<sub>2</sub>O<sub>3</sub> in their test rig. The calculated recession rates were in the range of 2.94·10<sup>-10</sup> g·cm<sup>-2</sup>·s<sup>-1</sup> for laminar flow and 1.99·10<sup>-10</sup> g·cm<sup>-2</sup>·s<sup>-1</sup> for turbulent flow. Compared to those values, the calculated recession rates for this test rig are an order of magnitude higher, this is due to the higher gas velocities and the slightly higher temperature.

Table 3: Values for equations 5 and 6 and calculated recession rates.

		Y <sub>2</sub> O <sub>3</sub>	Al <sub>2</sub> O <sub>3</sub>	Reference
ρ (T)	g∙cm <sup>-3</sup>	9.10·10 <sup>-5</sup>	9.10·10 <sup>-5</sup>	ideal gas law
U	cm⋅s <sup>-1</sup>	2.24·10 <sup>5</sup>	2.24·10 <sup>5</sup>	CEA calculation
L	cm	1.6	1.6	Specimen radius
μ	g·cm <sup>-1</sup> ·s <sup>-1</sup>	5.07·10 <sup>-4</sup>	5.07·10 <sup>-4</sup>	[44]
$D_{AB}$	cm <sup>2</sup> ·s <sup>-1</sup>	2.16	2.655	[14]
ho'(T)	g∙cm <sup>-3</sup>	2.59·10 <sup>-12</sup>	5.12·10 <sup>-10</sup>	ideal gas law, [11]
<b>Ø</b> H2O	Å	2.641	2.641	[46]
$\sigma$ Gas	Å	4.198	5.127	[27, 46]
<b>ε</b> H2O / <b>k</b>	K	809.1	809.1	[46]
<b>ε</b> Gas /k	K	1846	472	[27, 46]
Ω		1.261	0.83	[48]
$oldsymbol{J}$ laminar	g·cm <sup>-2</sup> ·s <sup>-1</sup>	8.08-10 <sup>-10</sup>	1.84·10 <sup>-7</sup>	
<b>J</b> turbulent	g·cm <sup>-2</sup> ·s <sup>-1</sup>	1.24·10 <sup>-9</sup>	2.81·10 <sup>-7</sup>	

## Corrosion Tests with Ox/Ox CMC

Corrosion tests of the alumina CMCs were carried out with 10, 20 and 40 min test durations. Figure 4 depicts the topographic images of ox/ox CMCs before and after corrosion testing. Even after such short test duration, a clear effect on the surface topography of the sample can be observed. The topography images show that the flame hits the substrate precisely at one spot. A maximum depth of 200 µm of the resulting corrosion damage was measured.

The mass losses with respect to the initial sample weight are given in Figure 5. The measured mass losses of the individual test series are close together, implying a good reproducibility. A corrosion rate of  $2.32 \pm 0.2 \, \text{mg} \cdot \text{g}^{-1} \cdot \text{h}^{-1}$  was measured. The measured mass loss was used to calculate the area-related recession rate. The geometric dimensions of the sample were used to calculate the surface area, even though this leads to a drastic underestimation of the real surface as porosity and roughness are neglected. A recession rate of  $5.56 \cdot 10^{-7} \, \text{g} \cdot \text{cm}^{-2} \cdot \text{s}^{-1}$  was calculated. This result is in the same order of magnitude as the calculated recession rate for  $\text{Al}_2\text{O}_3$  in this test rig.

The measured corrosion rate is compared to the corrosion rates of alumina that were found by other groups in Table 4. For comparison, the literature corrosion rates were converted to the present test conditions with the corresponding fluxes.

It is noticeable that the recalculated corrosion rate for OPILA et al. is the highest among the calculated corrosion rates, although the initially measured corrosion rate

was at least one order of magnitude smaller than the other corrosion rates. This might be due to the test conditions of this setup. Since OPILA et al.<sup>[11]</sup> tested in a quasi-stationary atmosphere, which leads to a very low flux. Due to the long test duration and the quasi-stationary atmosphere, it can be assumed that the thermodynamic equilibrium is present and the removal of the volatile hydroxide is the rate-determining step. The other test rigs worked with significantly higher velocities and thus higher fluxes. With increasing velocity, however, the rate-determining step shifts. It can be assumed that at supersonic gas velocities the hydroxide formed on the surface is immediately removed by the gas flow. As a consequence, the corrosion rate is determined by the reaction rate of the volatile species itself. The corrosion rates presented in this study are quite high, compared to the other literature values<sup>[15, 24]</sup> for dense Al<sub>2</sub>O<sub>3</sub>. There are several possible reasons for that:

Due to the open porosity of 29 %, the effective surface that can be attacked by water vapor is considerably higher than the geometric surface (7 m² vs. 8 cm²). As dense samples were used in most tests found in the literature, this could have drastic influence on the calculated corrosion rate. Moreover, porous samples are more susceptible to erosion than dense samples, but erosion would also occur in a turbine, which makes the test more realistic. Finally, the extremely high flow rate drastically increases the reaction rate. According to equations 12 and 13 a higher gas flow leads to higher corrosion rates.

Table 4: Test conditions and measured corrosion rates of  $Al_2O_3$  of literature known test rigs compared to the HVOF-test rig. For a better comparison, the measured recession rates were converted to the present test conditions.

Author	Temperature (°C)	P <sub>H2O</sub> (%)	Time (h)	Gas Velocity (m/s)	Recession Rate (mg·cm <sup>-2</sup> ·h <sup>-1</sup> )	Recalculated Recession Rate (mg·cm <sup>-2</sup> ·h <sup>-1</sup> )
OPILA <sup>[11]</sup>	1400	50	100	0.044	0.002	10.94
FRITSCH <sup>[24]</sup>	1450	28	500	100	0.03	1.37
Yuri <sup>[15]</sup>	1500	9	20	40-250	0.07	0.22
This study	1400	69	0,67	2600	2.14	2.14

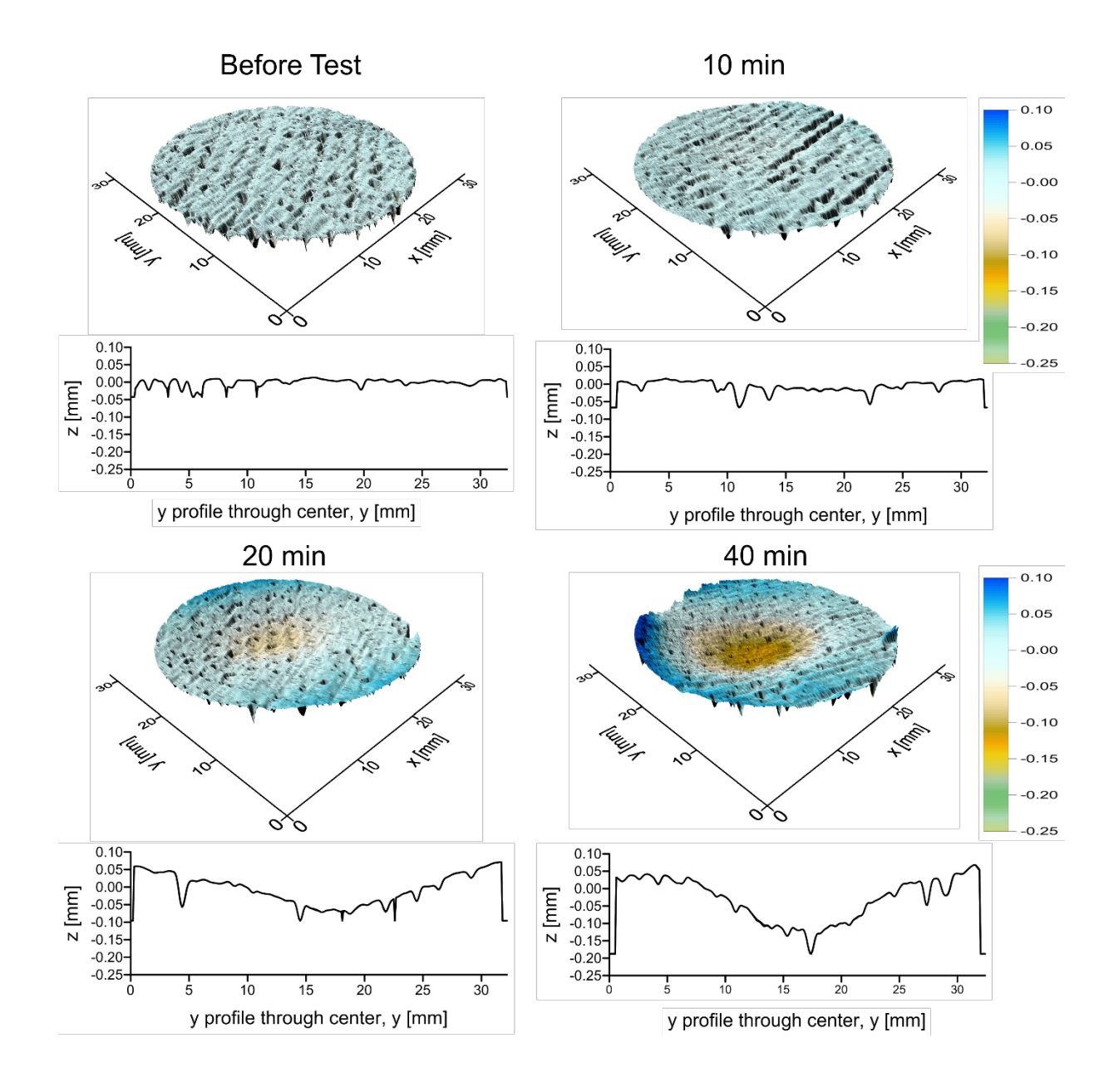


Figure 4: Sample topography measured with white light interferometry of uncoated CMC samples before and after HVOF corrosion test.

The thickness reduction of the substrates which would arise from homogeneous one dimensional recession of the CMCs was estimated from the measured mass loss in the 40 min experiments for two extreme scenarios:

First, the maximum thickness reduction was estimated using the geometric dimensions and the density of the sample. Neglecting both, the high porosity of the

sample and its roughness, is expected to lead to a drastic over estimation of the recession depth. The calculation (see equation 14) results in an area of  $804 \text{ mm}^2$  for the samples front side, resulting in a maximum recession depth of  $5.18 \mu m$ .

$$\frac{\textit{mass loss}}{\textit{density-surface area}} = \frac{0.012g}{2.88 \frac{g}{\textit{cm}^3} \cdot 8.04 \; \textit{cm}^2} = 5.18 \; \mu m \tag{14}$$

Second, the minimum recession depth was calculated using the full accessible surface area. The accessible surface area was measured by BET measurements, an area of  $2.538~\text{m}^2\cdot\text{g}^{-1}$  was measured. This leads to a surface of  $17.5~\text{m}^2$  per sample. The total surface values were corrected in a way that only the fraction of the front side is taken into account (42.5% of the total surface). This results in a maximum surface area of  $7.5~\text{m}^2$  and a corresponding minimum expected recession depth of  $5.6\cdot10^{-4}~\mu\text{m}$ .

It is noticeable that both values are clearly below the measured profile change. The profile deviations are probably caused by bending of the specimens, which is due to stresses induced by the thermal gradient and clamping of the specimen during the test.

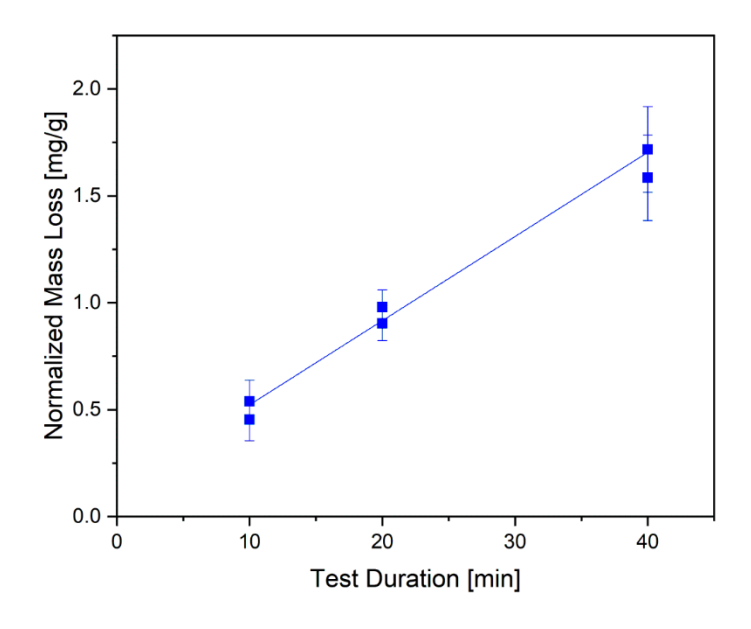


Figure 5: Linear increase of mass loss of Al<sub>2</sub>O<sub>3</sub> CMC with increasing test duration.

In order to clarify whether corrosion or erosion is the reason for the mass loss, the sample surfaces were examined more closely. SEM-images of CMC samples before and after testing are shown in Figure 6. The sample surface looks homogenous before testing. Fine YSZ particles of about 100 nm size (bright contrast compared to aluminum oxide in SEM images) are homogeneously distributed in the porous matrix of the aluminum oxide particles in sizes up to several micrometers. After 40 minutes of testing, the surface morphology is coarser. The coalescence of the particles can be attributed to sintering during heat treatment. The relative amount of YSZ phase seems to have increased. Alumina is less corrosion resistant than YSZ, so it is attacked first, resulting in an alumina depleted surface layer.

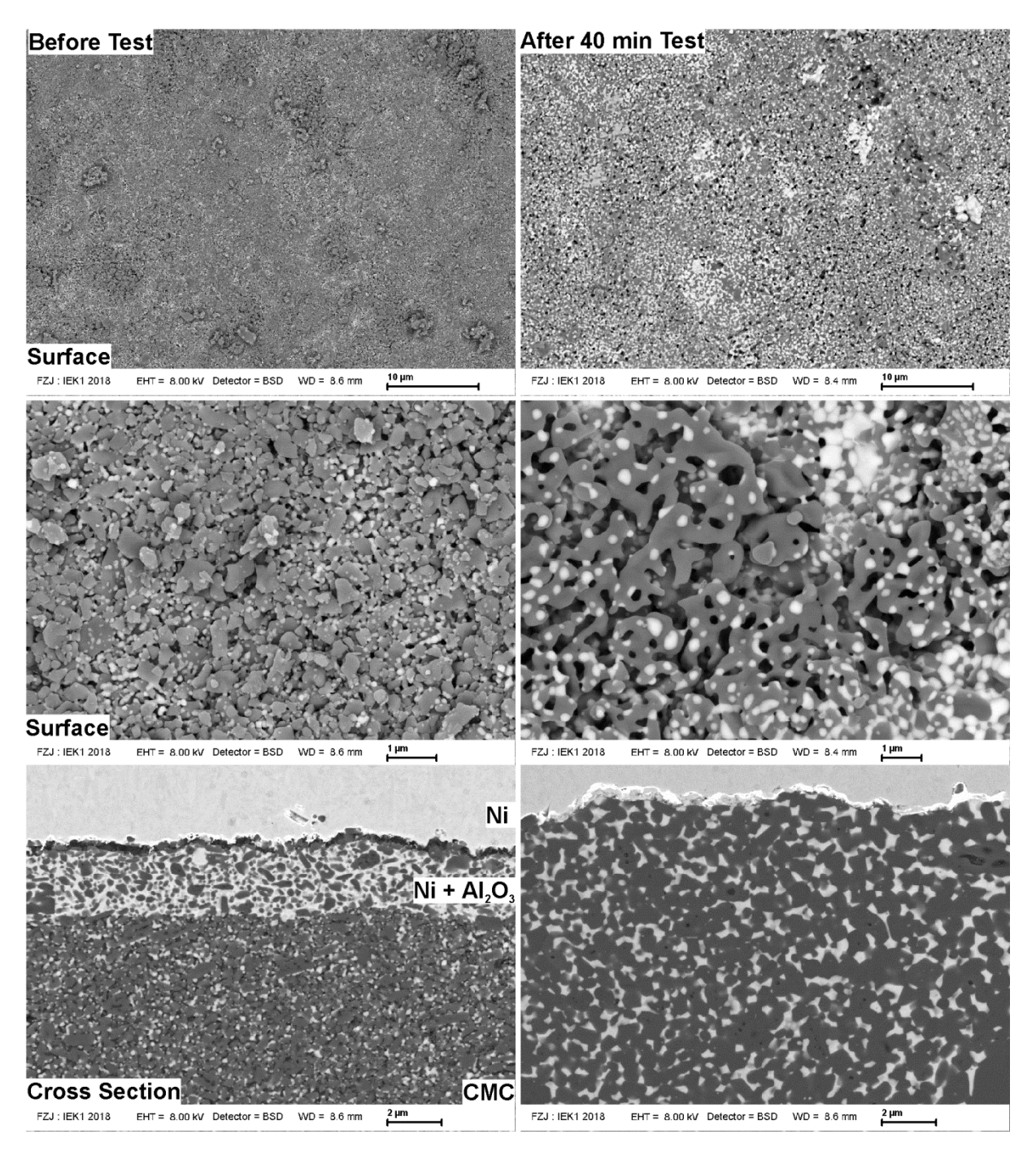


Figure 6: SEM-Image of the uncoated CMC before (left) and after 40 minutes of HVOF-testing (right).

Afterwards cross sections were made. The specimens were previously electroplated with nickel to protect the surface during sample preparation and to shift the gap between sample and resin away from the area of interest. The SEM images of the polished cross sections are shown in Figure 6 (bottom). It can be seen that

significant sintering took place during the experiment. The thermal treatment leads to a noteworthy grain growth and densification of the samples surface. Thus the nickel could penetrate about 2  $\mu$ m deep into the CMC before the test, while no nickel-CMC mixing zone was found in the cross section after the test. The calculations of the corrosion depth suggested changes on a very small scale (nanometer range), which is hard to visualize by SEM. So it is not surprising that the traces of corrosion cannot be seen inside the sample, as the corrosion is mainly limited to the samples surface.

EDX measurements were performed on the samples surfaces before and after corrosion test. The Al/Zr ratio was used to analyze the corrosion resistance of the samples; the results are illustrated in Figure 7. For the used material, the Al/Zr ratio should be in the range of 3.6, according to the manufacturer. The EDX results proved a mean Al/Zr ratio of 3.7 ±1.1, which corresponds to the theoretical value almost exactly. After 40 min of water vapor corrosion this ratio is nearly reduced by 50%. This can be explained by the higher recession rate of alumina compared to YSZ. During the test, alumina is removed and the more stable matrix additive (YSZ) remains, resulting in a reduction of the Al/Zr ratio. Although additional deviations from the actual concentration ratios may occur from the limits of the EDX evaluations of rough surfaces, the results give further indications of the already assumed preferred corrosion of Al<sub>2</sub>O<sub>3</sub>.

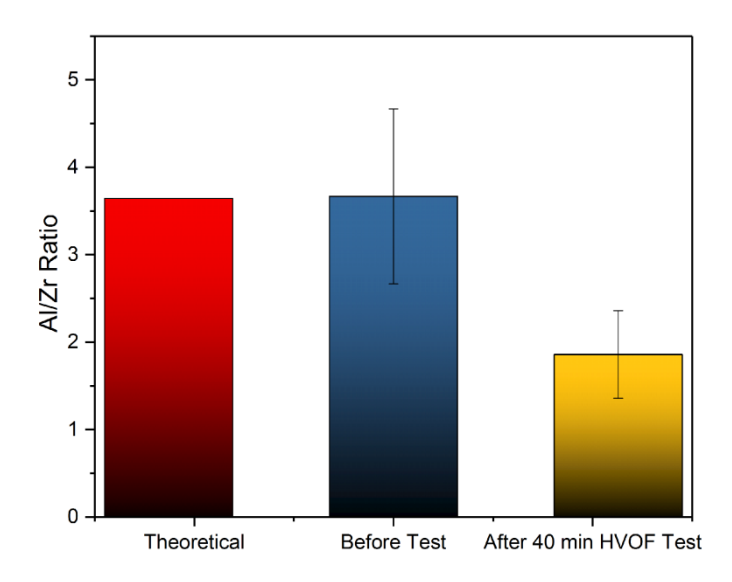


Figure 7: Results of EDX measurements on sample surfaces before and after corrosion.

Rietveld refinements (Figure 8) of XRD patterns measured before and after 40 min corrosion test, with glazing incidence method, showed the same trend. It was found that the alumina content at the surface is decreased from 85 % to 77 % after the test. The YSZ content on the surface is increased accordingly. The Al/Zr ratio was calculated on the basis of these refinements (Al/Zr=2.15), and was found to correspond to the values determined by EDX  $(1.9 \pm 0.5)$  within the errors. This further indicates that corrosion of alumina took place on the surface.

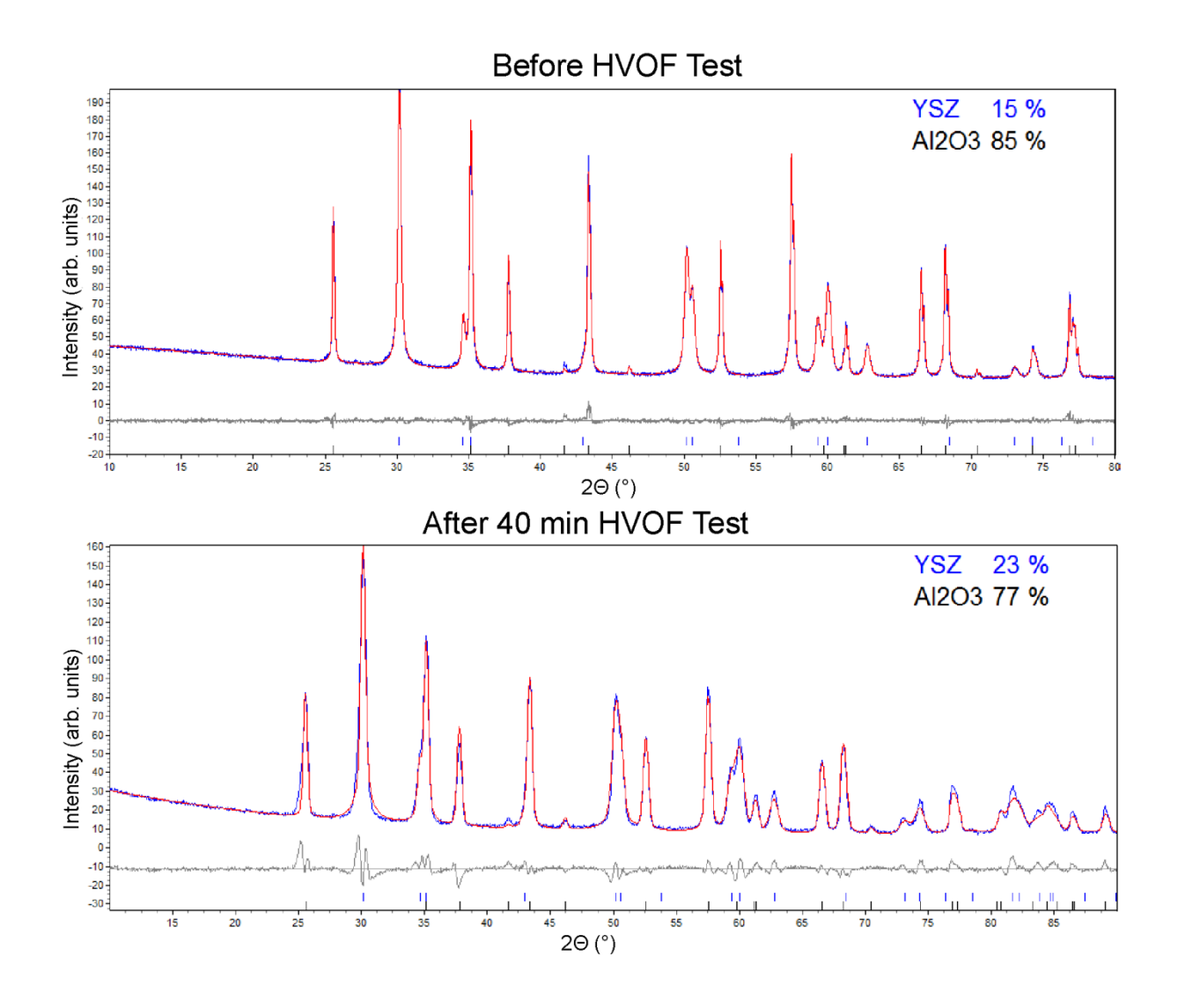


Figure 8: XRD-Measurements of samples before (top) and after (bottom)

HVOF-test, measured signal (blue), refinement (red), difference plot (grey).

### Corrosion Tests with Y<sub>2</sub>O<sub>3</sub>-EBC

The test durations for the runs with coated samples were 20 and 40 min. The white light interferometry scans are shown in Figure 9. As one can see the surface is less affected by the test, compared to the uncoated CMC samples. The measured mass losses as function of time are shown in Figure 10. Table 6 presents the mean mass losses and corrosion rates of all test runs.

Corrosion rates of  $0.67 \pm 0.2$  mg·g<sup>-1</sup>·h<sup>-1</sup> were measured. The measured corrosion rate is compared to literature values in Table 5. The literature values differ significant from another, therefore the different rates are hard to compare. The measured mass loss leads to an area-related corrosion rate of Y<sub>2</sub>O<sub>3</sub> is  $4.47 \cdot 10^{-7}$  g·cm<sup>-2</sup>·s<sup>-1</sup>, compared to the calculated rate of  $1.24 \cdot 10^{-9}$  g·cm<sup>-2</sup>·s<sup>-1</sup> this value is quite high. The difference between the calculated and the measured value can be explained by the removal of loose powder residues at the beginning of the test and by the strongly simplified calculations. Furthermore, the surface area was calculated using the geometric dimensions of the sample, which completely neglects surface texturing, roughness and porosity and leads to a drastic overestimation of the corrosion rate.

A summary of all tested samples is given in Figure 10 and Table 6. The normalized mass loss of Y<sub>2</sub>O<sub>3</sub> coated CMCs increases significantly slower over time compared to uncoated CMCs, indicating an inhibitory effect. As in the previous tests, the results show only a minor scatter, which shows the good reproducibility of the

tests. The corrosion rate of the coated CMC as derived from the slopes in linear fitting is decreased by a factor of four when compared to the uncoated CMC.

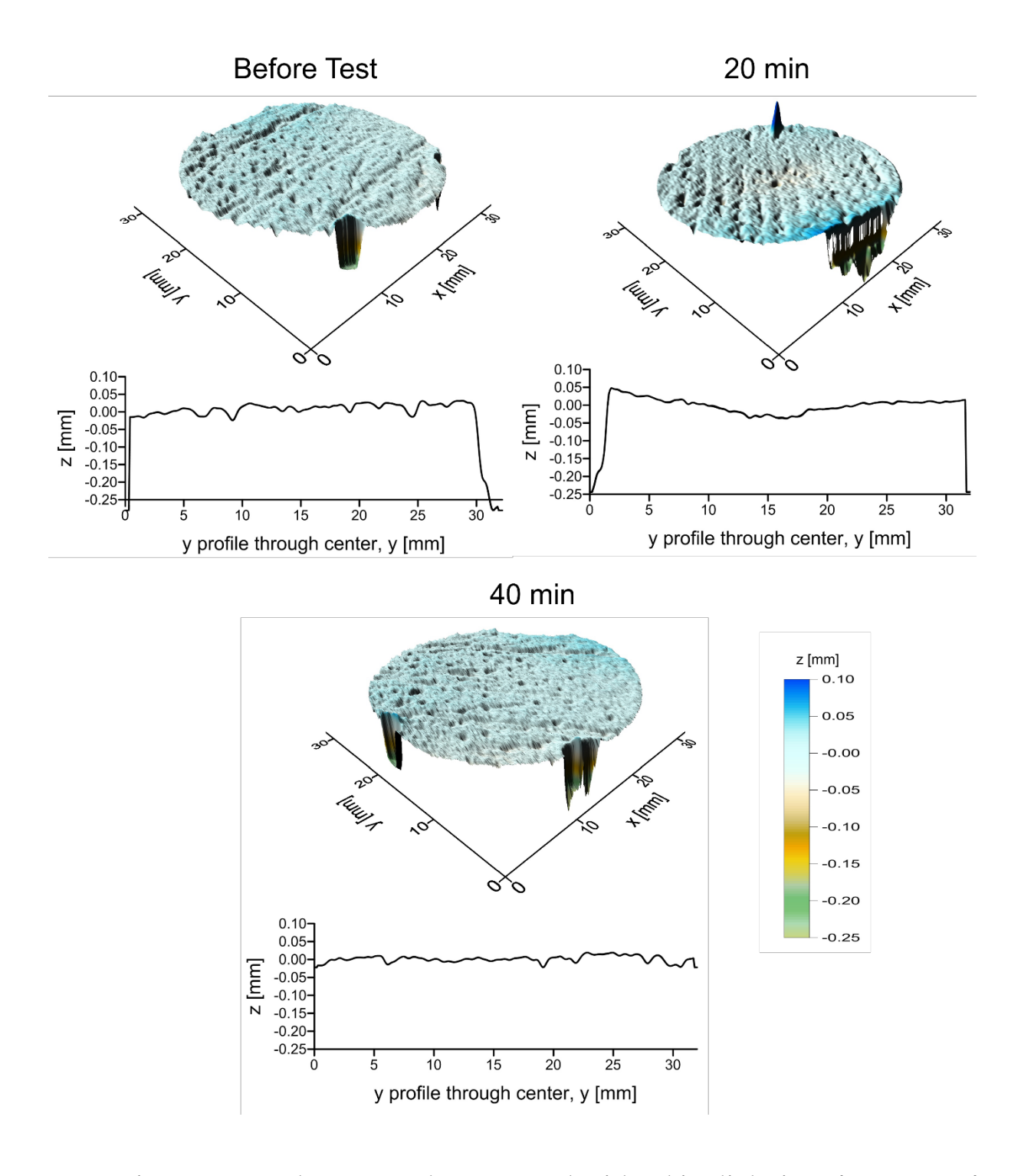


Figure 9: Sample topography measured with white light interferometry of coated CMC samples before and after HVOF corrosion test.

Table 5: Test conditions and measured corrosion rates of Y<sub>2</sub>O<sub>3</sub> of literature known test rigs compared to the HVOF-test rig. For a better comparison, the measured recession rates were converted to the present test conditions by the corresponding flux.

Author	Temperature (°C)	P <sub>H2O</sub> (%)	Time (h)	Gas Velocity (m/s)	Recession Rate (mg·cm <sup>-2</sup> ·h <sup>-1</sup> )	Recalculated Recession Rate (mg·cm <sup>-2</sup> ·h <sup>-1</sup> )
GOLDEN <sup>[27]</sup>	1300	100	80	177	1.4·10 <sup>-7</sup>	6.03·10 <sup>-7</sup>
Courcot <sup>[49]</sup>	1300	50	140	0.05	0.12	410
This study	1400	69	0,67	2600	1.6	1.6

Figure 10 shows that the y-axis intercept of the EBC system is not zero. This offset could be caused by remaining of loose powder owing to the coating process. These powder residues are removed by the high gas flow at the beginning of the test. This effect can be compensated with longer test times. This effect was also observed by FRITSCH et al.  $^{[12]}$  for tests with an Y<sub>3</sub>Al<sub>5</sub>O<sub>12</sub>-EBC. The measured graphs (300 h test duration) show similar trends as the ones in the present study after 40 min.

Table 6: Mean measured recession rates and weight loss of all test durations.

Test Duration	Normalized Mass	Mass Loss per	Recession Rate
(min)	Loss (mg/g)	Area (mg/cm²)	(mg/g·h)

**CMC** 

10	$0.50 \pm 0.04$	$0.42 \pm 0.03$	
20	0.94 ± 0.04	0.79 ±0.03	2.32 ± 0.20
40	1.65 ± 0.70	1.41 ± 0.08	
Y <sub>2</sub> O <sub>3</sub> coated CMC			
20	0.59 ± 0.10	0.57 ± 0.10	
40	0.817 ± 0.0002	1.12 ± 0.20	0.67 ± 0.20

SEM-Images of Y<sub>2</sub>O<sub>3</sub>-coated CMC-samples before and after corrosion are shown in Figure 11. The sample possesses a relatively smooth surface before the corrosion test, after testing the surface seems to be slightly attacked. Minor effects of water vapor corrosion can be seen, as the surface looks more porous and rougher after testing.

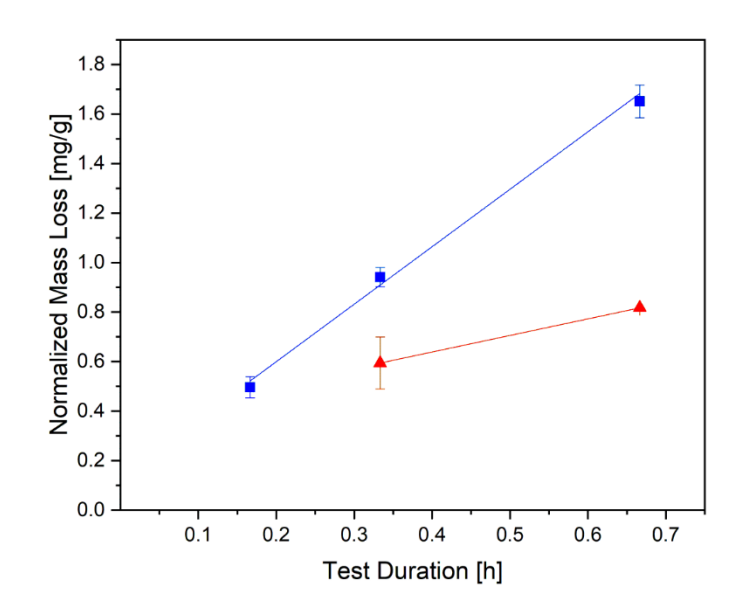


Figure 10: Summary of corrosion test results (blue squares: Al<sub>2</sub>O<sub>3</sub> CMC, red triangles: Y<sub>2</sub>O<sub>3</sub> coated CMCs).

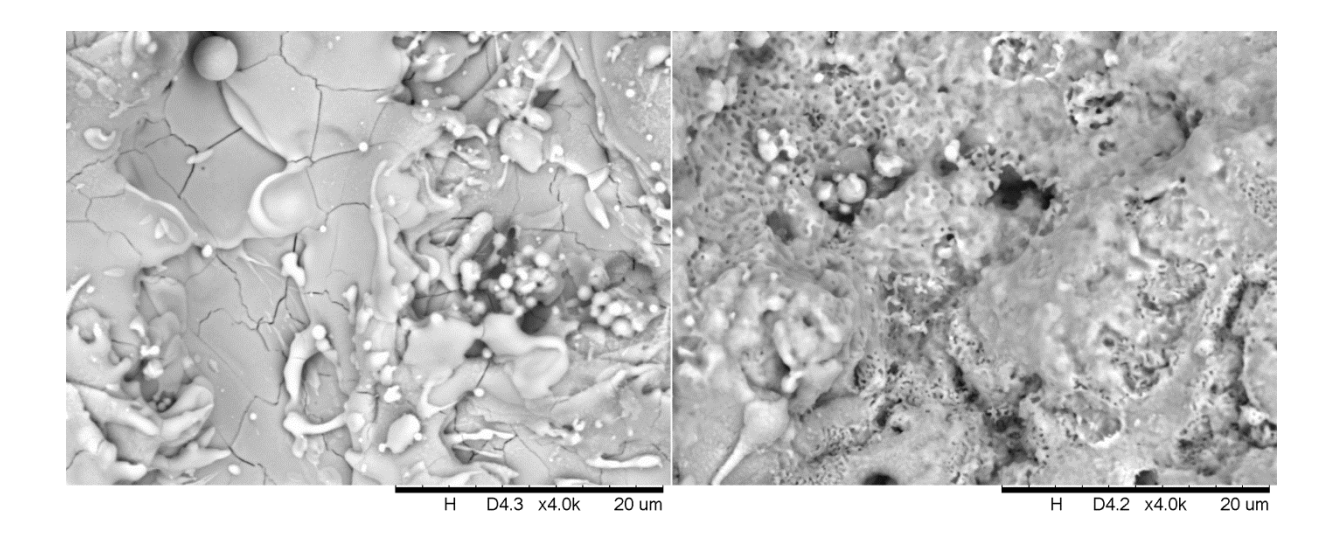


Figure 11: SEM-Image of the Y<sub>2</sub>O<sub>3</sub>-coated CMC before (left) and after 40 minutes of HVOF-testing (right).

### Conclusion

In summary, a new method of water vapor corrosion testing was presented. It was demonstrated that corrosion tests can be performed with an HVOF device, using hydrogen and oxygen as fuel gases. Calculations of the chemical equilibrium of the combustion reaction showed that a water partial pressure of nearly 70 kPa can be achieved. The flow velocity at sample position was roughly estimated to be around 2243 m·s<sup>-1</sup> at a total pressure of 0.1 MPa. Compared to other test facilities our test rig shows harsh conditions, especially high gas velocities.

The flux was used to compare the different test facilities. This showed that low pressures can easily be compensated by high gas velocities. The extremely high gas velocity and the high partial pressure of water vapor lead to the highest flux in our test rig in comparison with used test rigs in the literature.

The HVOF test rig was verified by several tests with uncoated Al<sub>2</sub>O<sub>3</sub>/Al<sub>2</sub>O<sub>3</sub>-CMCs and Y<sub>2</sub>O<sub>3</sub> coated CMCs. The corrosion behavior of coated and uncoated CMCs over different test durations showed a linear behavior. The porous, uncoated CMCs had the highest corrosion rates. EDX and XRD surface measurements showed a significant decrease of the alumina content. CMCs previously coated with an environmental barrier coating showed significantly lower corrosion rates with continuous testing time. This confirms the corrosion inhibiting effect of the EBC.

Within each test series, the measured mass losses showed only low scattering, so that a very good reproducibility of the HVOF corrosion test results could be

demonstrated. Deviations of the corrosion rates determined in this study compared to values reported in the literature for bulk ceramics are most reasonably attributed to the influence of the complex morphology of the CMC and EBC systems. A future adaption of the experimental setup to specimen of monolithic ceramics is expected to improve the link to other studies.

## Acknowledgement

The authors would like to thank Dr. G. Mauer for the support by the CEA calculations and Dr. Y. J. Sohn for carrying out the XRD analysis. Furthermore the authors would like to thank Dr. D. Sebold for the SEM recordings and Dr. H. Schlenz for the EDX measurements. We would like to thank S. Schwartz-Lückge for the measurement of the BET surfaces, as well as F. Kurze and K.-H. Rauwald for their support during the HVOF-tests. Further we would like to thank our partner institute, IEK-2, for the nickel plating of the samples.

### References

- [1] B. T. Richards, H. N. G. Wadley, "Plasma spray deposition of tri-layer environmental barrier coatings", *Journal of the European Ceramic Society* **2014**, 34, 3069-3083.
- [2] J. Göring, B. Kanka, M. Schmucker, H. Schneider, "A Potential Oxide/Oxide Ceramic Matrix Composite for Gas Turbine Applications", *ASME Turbo Expo* **2003**, 621-624.
- [3] W. Braue, P. Mechnich, "Tailoring protective coatings for all-oxide ceramic matrix composites in high temperature-/high heat flux environments and corrosive media", *Materialwissenschaft und Werkstofftechnik* **2007**, *38*, 690-697.
- [4] P. Mechnich, W. Braue, in *Design, Development, and Applications of Engineering Ceramics and Composites*, John Wiley & Sons, Inc., **2010**, pp. 285-293.
- [5] P. Mechnich, W. Braue, "Air plasma-sprayed Y<sub>2</sub>O<sub>3</sub> coatings for Al<sub>2</sub>O<sub>3</sub>/Al<sub>2</sub>O<sub>3</sub> ceramic matrix composites", *Journal of the European Ceramic Society* **2013**, *33*, 2645-2653.
- [6] Peter Mechnich, Wolfgang Braue, H. Schneider, "Multifunctional Reaction-Bonded Alumina Coatings for Porous Continuous Fiber-Reinforced Oxide Composites", *International Journal of Applied Ceramic Technology* **2004**, *1*, 343-350.
- [7] W. Krenkel, *Keramische Verbundwerkstoffe*, WILEY-VCH Verlag GmbH & Co. KGaA, Weinheim, **2003**.
- [8] N. Wiberg, A. Holleman, *Lehrbuch der Anorganischen Chemie, Vol. 102. Auflage*, De Gruyter, Berlin, Boston, **2008**.
- [9] J.D.Birchall, "High strength ceramics: Problems and possibilities", *Journal of Physics and Chemistry of Solids* **1988**, 49, 859-862.
- [10] E. J. Opila, N. S. Jacobson, "Volatile Hydroxide Species of Common Protective Oxides and Their Role in High Temperature Corrosion", *Electrochemica Science Proceedings* **1996**, *96*, 269-281.
- [11] E. J. Opila, D. L. Myers, "Alumina Volatility in Water Vapor at Elevated Temperatures", *Journal of the American Ceramic Society* **2004**, *87*, 1701–1705.
- [12] M. Fritsch, H. Klemm, "The water-vapour hot gas corrosion behavior of Al<sub>2</sub>O<sub>3</sub>-Y<sub>2</sub>O<sub>3</sub> materials, Y<sub>2</sub>SiO<sub>5</sub> and Y<sub>3</sub>Al<sub>5</sub>O<sub>12</sub>-coated alumina in A combustion environment", *Ceramic Engineering and Science Proceedings* **2006**, 27, 149-159.
- [13] M. Fritsch, H. Klemm, M. Herrmann, B. Schenk, "Corrosion of selected ceramic materials in hot gas environment", *Journal of the European Ceramic Society* **2006**, 26, 3557-3565.
- [14] R. E. Wilson, C. E. Wicks, J. R. Welty, Fundamentals of momentum, heat, and mass transfer, 2d ed. ed., Wiley, New York, 1976.

- [15] I. Yuri, T. Hisamatsu, "Recession Rate Prediction for Ceramic Materials in Combustion Gas Flow", *ASME Turbo Expo* **2003**, *GT2003-38886*, 633-642.
- [16] E. J. Opila, "Paralinear Oxidation of CVD Sic in Water Vapor", *Journal of the American Ceramic Society* **1997**, *80*, 197-205.
- [17] Y. Endo, T. Tsuchiya, Y. Furuse, "Corrosion Behavior of Ceramics for Gas Turbine Application Silicon-based structural ceramics", *CERAMIC TRANSACTIONS*, 42, 319-326.
- [18] E. J. Opila, "Oxidation Kinetics of Chemically Vapor-Deposited Silicon Carbide in Wet Oxygen", *Journal of the American Ceramic Society* **1994**, 77, 730–736.
- [19] Y. Etori, T. Hisamatsu, I. Yuri, Y. Yasutomi, T. Machida, K. Wada, "Oxidation Behavior of Ceramics for Gas Turbines in Combustion Gas Flow at 1500°C", *ASME 1997 International Gas Turbine and Aeroengine Congress and Exhibition* **1997**, V004T013A015.
- [20] K. G. Nickel, "Corrosion of non-oxide ceramics", *Ceramics International* **1997**, 23, 127-133.
- [21] M. Fritsch, H. Klemm, "The water vapor hot gas corrosion of MGC materials with Al<sub>2</sub>O<sub>3</sub> as a phase constituent in a combustion atmosphere", *Journal of the European Ceramic Society* **2008**, *28*, 2353-2358.
- [22] M. Fritsch, H. Klemm, M. Herrmann, A. Michaelis, B. Schenk, "The water vapour hot gas corrosion of ceramic materials", *Ceramic Forum International* (Berichte der Deutschen Keramischen Gesellschaft) **2010**, 87, 11-12.
- [23] M. Herrmann, H. Klemm, "Corrosion of Ceramic Materials", *Comprehensive Hard Materials* **2014**, 2, 413-446.
- [24] M. Fritsch, Heißgaskorrosion keramischer Werkstoffe in H2O-haltigen Rauchgasatmosphären, Fraunhofer IRB Verlag, TU Dresden, **2007**.
- [25] Rüdinger, W. Pritzkow, "Die Entwicklung A. oxidkeramischer Zentrum Faserverbundwerkstoffe Fraunhofer **ISC** am / Zusammenarbeit mit W.E.C. Pritzkow Spezialkeramik", Keramische Zeitschrift **2013**, *03*, 166-169.
- [26] Walter E. C. Pritzkow Spezialkeramik, "Oxidkeramischer Faserverbundwerkstoff "Keramikblech", Neuentwicklungen für den Einsatz bis 1300 °C".
- [27] R. A. Golden, E. J. Opila, "A method for assessing the volatility of oxides in high-temperature high-velocity water vapor", *Journal of the European Ceramic Society* **2016**, *36*, 1135-1147.
- [28] S. L. dos Santos e Lucato, O. H. Sudre, D. B. Marshall, "A Method for Assessing Reactions of Water Vapor with Materials in High-Speed, High-Temperature Flow", *Journal of the American Ceramic Society* **2011**, *94*, s186-s195.

- [29] S. Gordon, B. J. McBride, Computerprogram for Calculation of Complex Chemical Equilibrium Compositions and Applications I. Analysis, NASA, **1994**.
- [30] B. J. McBride, S. Gordon, Computer Program for Calculation of Complex Chemical Equilibrium Compositions and Applications II. Users Manual and Program Description, NASA, 1996.
- [31] K. L. More, P. F. Tortorelli, M. K. Ferber, J. R. Keiser, "Observations of Accelerated Silicon Carbide Recession by Oxidation at High Water-Vapor Pressures", *Journal of the American Ceramic Society* **2000**, *83*, 211–213.
- [32] B. Sudhir, R. Raj, "Effect of Steam Velocity on the Hydrothermal Oxidation/Volatilization of Silicon Nitride", *Journal of the American Ceramic Society* **2006**, *89*, 1380-1387.
- [33] D. S. Fox, E. J. Opila, Q. N. Nguyen, D. L. Humphrey, S. M. Lewton, "Paralinear Oxidation of Silicon Nitride in a Water-Vapor/Oxygen Environment", *Journal of the American Ceramic Society* **2003**, *86*, 1256–1261.
- [34] D. Filsinger, A. Schulz, S. Wittig, C. Taut, H. Klemm, G. Wötting, "Model Combustor to Assess the Oxidation Behavior of Ceramic Materials Under Real Engine Conditions", *ASME* 1999 International Gas Turbine and Aeroengine Congress and Exhibition 1999, 4, V004T002A013.
- [35] H. Klemm, "Corrosion of silicon nitride materials in gas turbine environment", *Journal of the European Ceramic Society* **2002**, 22, 2735–2740.
- [36] R. C. Robinson, J. L. Smialek, "SiC Recession Caused by SiO<sub>2</sub> Scale Volatility under Combustion Conditions: I, Experimental Results and Empirical Model", *Journal of the American Ceramic Society* **1999**, *82*, 1817–1825.
- [37] E. J. Opila, "Oxidation and Volatilization of Silica Formers in Water Vapor", *Journal of the American Ceramic Society* **2003**, *86*, 1238–1248.
- [38] E. J. Opila, D. L. Myers, "Alimina Volatility in Water Vapor at Elevated Temperatures: Application to Combustion Environments", *Electrochemical Society Proceedings* **2003**.
- [39] M. K. Ferber, H. T. Lin, V. Parthasarathy, W. Brentnall, "Degradation of Silicon Nitrides in High Pressure, Moisture Rich Environments", *ASME* 1999 *International Gas Turbine and Aeroengine Congress and Exhibition* **1999**.
- [40] H. E. Eaton, G. D. Linsey, K. L. More, J. B. Kimmel, J. R. Price, N. Miriyala, "EBC Protection of SiC/SiC Composites in the Gas Turbine Combustion Environment", *ASME Turbo Expo 2000: Power for Land, Sea, and Air* **2000**, *4*, V004T002A018.
- [41] T. Fukudome, S. Tsuruzono, W. Karasawa, Y. Ichikawa, "Development and Evaluation of Ceramic Components for Gas Turbine", *ASME Turbo Expo* 2002: *Power for Land, Sea, and Air* **2002**, *4*, 135-140.

- [42] T. Fukudome, S. Tsuruzono, T. Tatsumi, Y. Ichikawa, T. Hisamatsu, I. Yuri, "Development and Evaluation of Ceramic Components for a Gas Turbine", *Key Engineering Materials* **2006**, *317-318*, 481-486.
- [43] K. L. More, P. F. Tortorelli, L. R. Walker, "High-Temperature Stability of SiC-Based Composites in High-Water-Vapor-Pressure Environments", *Journal of the American Ceramic Society* **2003**, *86*, 1272–1281.
- [44] B. Latto, "Viscosity of steam at atmospheric pressure", *International Journal of Heat and Mass Transfer* **1965**, *8*, 689.
- [45] G. H. Geiger, D. R. Poirier, *Transport phenomena in materials processing*, Minerals, Metals and Materials Society, Warrendale, Pa., **1994**.
- [46] R. A. Svehla, *Estimated viscosities and thermal conductivities of gases at high temperatures*, *Vol. R-132.*, National Aeronautics and Space Administration, Washington, **1963**.
- [47] O. H. Krikorian, "Predictive calculations of volatilities of metals and oxides in steam-containing environments", *High Temperatures High Pressures* **1982**, *14*, 387-397.
- [48] R. B. Bird, C. F. Curtiss, J. O. Hirschfelder, *Molecular theory of gases and liquids*, Corr. print. with notes added. ed., Wiley, New-York, NY, **1967**.
- [49] E. Courcot, F. Rebillat, F. Teyssandier, C. Louchet-Pouillerie, "Stability of rare earth oxides in a moist environment at high temperatures—Experimental and thermodynamic studies. Part I: The way to assess thermodynamic parameters from volatilisation rates", *Journal of the European Ceramic Society* **2010**, *30*, 1903-1909.